Spatial and Temporal Infiltration Dynamics during Managed Aquifer Recharge

ANDREW J. RACZ,[1] ANDREW T. FISHER,[1] CALLA S. SCHMIDT,[1] BRIAN S. LOCKWOOD,[2] MARC LOS HUERTOS[3]

[1]University of California, Santa Cruz, Santa Cruz, California 95064

[2]Pajaro Valley Water Management Agency, Watsonville, California 95076

[3]California State University, Monterey Bay, Seaside, California 93955

1

Abstract. Natural groundwater recharge is inherently difficult to quantify and predict, largely because it comprises a series of processes that are spatially distributed and temporally variable. Infiltration ponds used for managed aquifer recharge (MAR) provide an opportunity to quantify recharge processes across multiple scales under semi-controlled conditions. We instrumented a three-hectare MAR infiltration pond to measure and compare infiltration patterns determined using whole-pond and point-specific methods. Whole-pond infiltration was determined by closing a transient water budget (accounting for inputs, outputs, and changes in storage), whereas point-specific infiltration rates were determined using heat as a tracer and time-series analysis at eight locations in the base of the pond. Whole-pond infiltration, normalized for wetted area, rose rapidly to >1.0 m/d at the start of MAR operations (increasing as pond stage rose), was sustained at high rates for the next 40 days, then decreased to <0.1 m/d by the end of the recharge season. Point-specific infiltration rates indicated high spatial and temporal variability, with the mean of measured values generally being lower than rates indicated by whole-pond calculations. Co-located measurements of head gradients within saturated soils below the pond were combined with infiltration rates to calculate soil hydraulic conductivity. Observations indicate a brief period of increasing saturated hydraulic conductivity, followed by a decrease of one to two orders of magnitude during the next 50-75 days. Locations indicating the most rapid infiltration shifted laterally during MAR operation, and we suggest that infiltration may function as a "variable source area" processes, conceptually similar to catchment runoff.

Introduction and Project Motivation

Groundwater is essential for meeting fresh water demand worldwide, to satisfy urban, agricultural, industrial, and environmental needs, particularly in arid and semi-arid parts of the western and southern United States. In California, ~40% of fresh water demand is met by groundwater during a "normal" year (when hydrologic conditions are consistent with long-term averages), but during dry years, groundwater supplies up to ~60% of demand (California Water Plan Update 2009). Increasing population, continuing agricultural and municipal development, and anticipated changes to the regional hydrologic

cycle (especially the intensity, location, and seasonal variability of precipitation) all pose challenges for the successful management of water resources; resource managers in many regions will rely more heavily on groundwater in coming decades.

Many groundwater basins in California are overdrafted, such that the combined influence of groundwater pumping and the sum of other inputs and outputs has led to unacceptable harm to environmental resources and systems (Harou and Lund 2008; Fleckenstein et al. 2004; Reinelt 2005). Groundwater overdraft can lead to land subsidence (and an associated loss of storage capacity), seawater intrusion, reductions in baseflow to streams (sometimes leading to the formation of dry gaps), and reductions in surface water and groundwater quality and the health of aquatic habitat (Gallardo et al. 2009; Werner and Simmons 2009; Zektser, Loaiciga, and Wolf 2005; Harvey, Ayers, and Gosselin 2007). To address threats to the environment and water supply associated with overdraft, artificial recharge of groundwater is gaining popularity as a water management tool in California and throughout the world.

Artificial recharge comprises a series of strategies and techniques for increasing the flow of water into an aquifer, often using excess flows in streams or other surface channels, agricultural return flows, or treated wastewater (Bouwer 2002; Prommer and Stuyfzand 2005; Massmann et al. 2008; Greskowiak et al. 2005). Recharge can be achieved using injection wells, bank filtration in streams, and infiltration ponds. Artificial recharge achieved using surface infiltration basins is commonly referred to as "managed aquifer recharge" (MAR). Successful application of MAR generally requires maintaining relatively high hydraulic conductivity in shallow soils, so that infiltration conveys water efficiently from the surface to the subsurface during regular periods of system operation. Rates of infiltration during MAR are often rapid initially, but infiltration generally slows over time during periods of system operation as a result of physical, chemical, and biological processes (Bouwer, Ludke, and Rice 2001).

MAR projects are often operated in arid to semiarid climates, where there is a thick vadose zone between the infiltration basin and the underlying aquifer (Izbicki, Flint, and Stamos 2008; Heilweil, Solomon, and Gardner 2007). In some cases, the depth to the regional water table is tens to hundreds of meters. Where there is a thick vadose zone, the soil above the water table may never become fully saturated, even during long periods of MAR operation. Instead, a localized saturated zone with an "inverted water table" will form beneath the infiltration pond, and a thicker layer of largely unsaturated conditions will remain between the inverted water table and the regional water table, even as infiltrating water flows rapidly downward. Groundwater flow in this soil zone occurs either as unsaturated flow, governed by the physics of multiphase transport, or as saturated flow along spatially limited, preferential flow paths.

Not all of the water infiltrated during MAR becomes recharge. Some infiltration becomes trapped in the vadose zone as soil water, particularly infiltration that occurs near the start of the MAR operation season, and can be returned to the atmosphere by evaporation and transpiration. Quantifying MAR infiltration is an important step in determining the contribution of MAR to improving groundwater resources, and generally provides an upper limit on the extent of recharge. In addition, researchers and water managers need to understand the distribution of infiltration within MAR ponds, spatially and temporally, so as to resolve the extent of causes of reductions to MAR efficiency. This is particularly important if MAR is linked to low-impact development, stormwater capture, passive discharge from adjacent waterways, or other mechanisms that make it difficult to accurately determine the rate of inflow to a MAR infiltration system. Resolving temporal and spatial variability in infiltration is also important for quantifying the influence of MAR on the delivery of nutrients and other contaminants to underlying aquifers, and associated changes to groundwater quality, and provides insight as to the nature of infiltration and recharge processes in general.

In this study, we compare whole-system and point-specific infiltration rates and their spatial and temporal variability within an operating MAR recharge pond. Whole-system and point-specific infiltration rates were determined using mass balance and time-series thermal techniques, respectively. Point-specific infiltration rates were combined with independent measurements of saturated pressure gradients to quantify the magnitudes, locations, and timing of changes to the hydraulic conductivity of shallow soils at the field site. Additional studies are exploring the processes responsible for spatial and temporal heterogeneity in infiltration and hydraulic conductivity reported in the present study, and quantifying the influence of MAR infiltration on groundwater quality (Schmidt et al. 2011).

Experimental Site and Methods

This study focuses on samples and data collected during the 2007–08 water year (1 October 2007 – 30 September 2008) in and around the Harkins Slough MAR (HS-MAR) pond, an infiltration basin on the western side of the Pajaro Valley, central coastal California (Figure 1). The recharge pond has an area of three hectares and occupies a modified natural depression overlying Holocene alluvial and fluvial deposits and dune sands (Hanson 2003). Annual precipitation across the Pajaro Valley averages 50 cm/yr, with >90% of precipitation falling between December and April. Many streams and wetlands in this region fill and flood during the rainy season, but become dry later during the water year.

The HS-MAR project is operated by the Pajaro Valley Water Management Agency (PVWMA), which is permitted to divert up to 2.5×10^6 m^3 of surface runoff from Harkins Slough during the rainy season when slough levels and water quality are sufficiently high. Water diverted from the slough is passed through a sand pack filter, then pumped through a 1.5 km pipeline to a MAR infiltration pond (Figure 1). The maximum water depth the MAR pond is ~6 m when the pond is full. Groundwater beneath the MAR pond is perched atop a fine-grained unit ~20–30 m below the ground surface. Before seasonal diversion from the slough begins, the local water table is ~15–20 m below the base of the pond. When the infiltration pond is filled and MAR peaks, groundwater levels in monitoring wells surrounding the

pond typically rise by 3–6 meters. Recovery wells adjacent to the pond are used to withdraw shallow groundwater, which is blended with other water supplies and distributed by pipeline to surrounding agricultural lands. Water supplied by the Harkins Slough MAR system allows reduced usage or retirement of coastal wells tapping a deeper, regional aquifer that is impacted by seawater intrusion.

The HS-MAR pond was surveyed, soils were sampled, and instruments were installed prior to the start of water diversion and infiltration in 2008. A digital elevation model (DEM) for the pond was created with a high-resolution laser scanning survey referenced to mean sea level (msl). Benchmarks located adjacent to the pond were used to determine relative and absolute elevations of instrument, sampling and monitoring points across the pond. Soils were collected using a hand auger to a maximum depth of 2.5 m below ground surface along a series of transects across the pond (Figure 1c). Soil samples were arranged on a sample description board in the field to recapitulate local stratigraphy, document color, classify texture, and note lithologic changes. Soil columns were photographed and subsampled (20-40 cm^3) for grain size, organic carbon, and other analyses at regular intervals. Soils grain size distribution was determined on selected samples following digestion in peroxide (to remove organic material), freeze drying, and homogenization to produce a representative mixture. Grain size analyses were completed with a Beckman Coulter LS 13320 laser diffraction particle size analyzer following suspension of digested soils in water and deflocculation with sodium metaphosphate. Soil porosity values were determined empirically based on grain size distribution data.

Whole pond infiltration rates were calculated by mass balance:

$$I = D + P - E - \Delta V \quad (1)$$

where net infiltration (I) comprises the sum of the following terms (all determined as positive values except as indicated below):

- Diversions (D) from Harkins Slough, measured hourly.

- Precipitation (P) into the pond, measured hourly on site with a tipping bucket rain gage, and verified using public records acquired from the California Irrigation Management Information System (CIMIS), Watsonville West Station #209, located 2.6 kilometers north of the field site. Although the pond is located within a natural depression, sandy soils in the region surrounding the pond have a high infiltration capacity, and we observed little hill-slope runoff into the pond,.
- Evaporation (E) from the pond, determined hourly at CIMIS Station #209, based on calculations of potential evapotranspiration (PET). In later project years we collected meteorological data at the HS-MAR pond (temperature, net solar radiation, wind speed) and compared longer term open water evaporation calculations (e.g., Winter et al., 1995) to CIMIS-derived PET values, with consistent results between these methods.
- Changes in storage in the pond (ΔV) were determined every 15 minutes using an autonomous pressure gauge deployed in a stilling well in combination with the pond DEM. Absolute pressure records were corrected for barometric variations, also measured on site, and related to pond volume, surface area, and wetted area based on field observations of pond stage combined with the pond DEM. Values of ΔV were positive when the pond volume increased, and negative when the pond value decreased.

HS-MAR water budget calculations were completed at 15 to 60 minute intervals, then combined to determine daily mean flow rates and storage changes, allowing for comparison with daily point-specific infiltration rates based on thermal methods, described later. Daily pond infiltration values (units of m^3/d) were normalized by wetted area (varies with pond stage) to derive specific infiltration rates for the whole pond (units of $m^3/m^2/d = m/d$). These values were divided by a porosity value typical of shallow soils below the pond to convert to average linear velocity, which allows a direct comparison between whole-pond and point-specific infiltration rates.

Point-specific infiltration rates within saturated soils below the HS-MAR pond were determined using heat as a tracer of fluid flow (Constantz, Thomas, and Zellweger 1994; Anderson 2005) based on time-series analysis of subsurface thermal data (Hatch et al. 2006). Daily fluctuations in the temperature at the base of the pond (typically 1–3 °C, even on cloudy days), propagate downward into the subsurface as thermal waves by conductive, advective, and dispersive processes. Daily temperature variations become reduced in amplitude and shifted in phase as they penetrate to greater depths (Figure 2), and the magnitude of amplitude reduction and phase shift are a function of infiltration rate. Time-series records of temperature below the pond are filtered to extract this diurnal signal, pairs of subsurface sensors are analyzed to resolve the amplitude reduction and phase shift once per day, and these values are used to solve for fluid infiltration rates based on a one-dimensional (vertical) conservation-of-heat equation. Application of this method depends on the spacing between pairs of subsurface sensors, not their absolute depths, so it is relatively insensitive to sedimentation or scour (e.g., a moving thermal boundary condition). This method has high sensitivity and a relatively wide dynamic range, being capable of quantifying rates from >10 m/d to <0.01 m/d (Hatch et al. 2006).

Subsurface thermal data were recorded at eight locations in 2008, as part of four instrument and soil/fluid sampling transects (Figure 1c). Autonomous thermal probes were deployed on cables suspended inside 3.8-cm diameter polyvinyl chloride (PVC) tubes. PVC tubes were screened at depths of ~70–90 cm below the base of the pond, so that they could also function as piezometers, and six of the tubes were instrumented with autonomous pressure loggers. Tubes were installed in boreholes excavated by hand auger, and a coarse sand filter (grain diameter = 0.7-1.7 mm, well rounded, >97% silica) was installed around the screen and capped with a 10 cm-thick bentonite seal. The shallow annulus of each borehole was backfilled with native soil, and a second bentonite seal was placed at the ground surface to prevent seepage along the sides of the tube. Following installation, piezometers were filled with water and developed by hand with a surge block to ensure good communication with the formation surrounding the screen, then instrumented with sensors. During normal MAR pond

180 operations, tubes remained filled with water when the depth of the inverted water table below the pond
181 base was below the base of the piezometer screens. Times when the soils around the screens were
182 unsaturated were readily apparent on temperature and pressure records. Thermal data from inside
183 piezometers are interpreted to be representative of conditions in adjacent soils when tubes were filled
184 with water, and infiltration rates were interpreted only when soils surrounding the sensors were
185 saturated. The relatively high thermal conductivity of water allows for this approach, provided there is a
186 good contact between the PVC tubing and the formation and that the sampling frequency is significantly
187 longer than the thermal time constant of the installation, in this case 5-6 minutes (e.g., Ronan et al.
188 1998; Constantz et al. 2001; Cardenas 2010).
189
190 Temperature was recorded at 15-minute intervals using autonomous sensors and data loggers having a
191 resolution of 0.02 ^{o}C, and pressure was measured at 30 minute intervals with a resolution of 0.04 kPa.
192 Filtering of time-series thermal records to resolve diel temperature variations results in resampling and
193 generation of a higher-resolution time series, with variations on the order of 0.001 °C being readily
194 apparent in processed records (Figure 2c, Hatch et al., 2006). Thermal loggers were deployed at depths
195 of ~20, 40 and 80 cm beneath the pond-sediment interface. Distances between thermal loggers were
196 measured to the nearest centimeter, as were geometrical parameters for each PVC tube (total depth,
197 screened depth, riser height). Ground surface elevations at each tube location were surveyed using a
198 laser totaling station and referenced to mean sea level, the same datum used to measure and record pond
199 stage. Processing of thermal data resulted in daily point-specific infiltration rates at each instrument
200 location.
201
202 **Results**
203 Shallow soils sampled from the upper 2.5 m below the base of the pond comprised 80–95% fine sand,
204 3–12% silt, and 1–7% clay. Most soils samples were classified as silty sand, although there were subtle
205 differences in grain size distribution across the pond and occasional thin layers distributed with depth

206 having somewhat higher contents of silt- and clay-sized material. Samples from Profiles 1 and 2 tended
207 to be the coarsest overall (generally <10% combined silt and clay), with slightly higher silt and clay
208 fractions found in samples from Profiles 3 and 4 (up to 20% silt and clay). Sediment porosity was
209 generally calculated to be 35-40%.
210
211 Daily water budget calculations show that diversions from Harkins Slough (*D*) comprised the greatest
212 source of inflow to the pond, reaching a maximum value near 2×10^4 m^3/d. Daily precipitation (*P*)
213 never exceeded 2% of daily diversions, and was <1% of total inputs for the vast majority of the MAR
214 operating period. Infiltration was the primary outflow from the pond, accounting for 98% of total season
215 inflows (*D* + *P*). Evaporation never exceeded 1% of infiltration until late in the operating period (after
216 day 110), when the rate of infiltration was greatly reduced.
217
218 Whole-pond mass balance calculations indicate that average specific infiltration rates were highest
219 during the first month of MAR operations, sometimes exceeding 1 m/d (Figure 3a). Infiltration rates
220 during this initial period correlate strongly with pond stage (R = 0.73, Figure 3b). Abrupt decreases in
221 the rate of diversions into the pond on operating days 12 and 25 correspond to rapid lowering of pond
222 stage and thus the hydraulic gradient driving infiltration. Later in the season, the pond stage and
223 infiltration rate became decoupled, with stage remaining relatively high and infiltration decreasing from
224 ~1.0 m/d to ~0.3 m/d, where it remained for the next 60 days. Stage dropped rapidly after seasonal
225 diversions ended around day 115, and whole-pond infiltration decreased to <0.1 m/d, where it remained
226 for the last 45 days of MAR operation (Figure 3a). There were multi-day variations in specific
227 infiltration rates measured between days 60 and 110, mainly as a result of how higher-resolution data
228 were aggregated to calculate daily infiltration values, but these variations were small in comparison to
229 longer-term trends.
230

231 Analyses of subsurface thermal records demonstrate that seepage was heterogeneous in time and space
232 across the bed of the MAR pond through the 2008 operating season. In most cases, infiltration at
233 individual thermal installations followed a pattern similar to that of the whole pond, with an initial
234 increase to a maximum infiltration rate, lasting 20–40 days, followed by a longer period of declining
235 infiltration rates (Figure 4a). Infiltration rates along Profile 1 (northwest end of the pond, Figure 1c)
236 were initially the greatest, rising rapidly to >1 m/d, but subsequently decreasing such that they were
237 below the whole pond infiltration rate after 15 days, and were the lowest measured by day 40. In
238 contrast, infiltration rates along Profile 4 (southeast end of the pond, Figure 1c) were initially just 0.2–
239 0.3 m/d, but rose slowly throughout the operating season, eventually reaching 0.6 m/d after 110 days of
240 infiltration. Infiltration rates along Profile 2, positioned between Profiles 1 and 4 (Figure 1c)
241 represented an intermediate case (Figure 4a). The daily means of all point-specific infiltration rates fall
242 below the whole-pond values by a factor of two to four. This suggests that the thermal probes were
243 disproportionately located in parts of the pond where infiltration rates were comparatively low.
244
245 Subsurface pressure records (corrected for local barometric pressure) illustrate how saturation
246 conditions varied throughout the 2008 MAR operating season (Figure 4b). Pressure rose most rapidly
247 during the first part of MAR operation and tracked pond stage most closely along Profile 4, where
248 infiltration was initially slowest. Pressure rose initially along Profiles 1 and 2 as well, but the start of the
249 pressure rise was delayed by several days and occurred more slowly, never reaching the peak observed
250 along Profile 4. This occurred in part because Profile 4 is in a deeper part of the pond (2.0–2.5 m deeper
251 than Profiles 1 and 2), but also indicates that it was more difficult to maintain saturated conditions along
252 Profiles 1 and 2 within the shallowest 1 m of soil. In fact, pressures became negative (less than
253 atmospheric) for brief periods early in the operating season along Profile 1, and late in the season along
254 Profile 2. Negative pressures occurred in soils below the pond when the rate of infiltration from above
255 was exceeded by the rate of deeper percolation, allowing the shallow soil to drain from below.
256 Sustaining negative pressures for brief periods below the pond also required that shallow, unsaturated

257 soils be decoupled from the atmosphere. Atmospheric pressures returned to Profile 1 after 50 days of
258 operation, indicating that unsaturated conditions extended to the edge of the pond in this area.
259
260 Subsurface pressure and pond stage records were combined during times when the shallow soils were
261 saturated to determine head gradients between the base of the pond and the screened depths of the
262 piezometers (center of screens ~80 cm below pond base) (Figure 4c). Some measured gradients,
263 particularly along the initially faster-infiltrating Profiles 1 and 2, were very large (approaching 10) and
264 nearly always exceed the canonical (steady-state) maximum natural value of 1 (Scanlon, Healy, and
265 Cook 2002). The elevated gradients likely resulted from a combination of high pond stage and low (but
266 positive) pressures in the shallow subsurface, when the transition from saturated to unsaturated
267 conditions occurred just below the piezometer screens.
268
269 We calculate daily, point-specific values of saturated soil hydraulic conductivity by combining
270 infiltration rates with subsurface head gradients, the same approach applied recently to streambed
271 measurements (Hatch et al. 2010) (Figure 4d). At all locations where we measured both infiltration rates
272 and head gradients, there was an initial period of rapidly increasing saturated hydraulic conductivity,
273 lasting 7-15 days, followed by a larger decrease in saturated conductivity lasting 50–75 days. The
274 subsequent conductivity decline was most rapid and extensive along Profile 1, where initial hydraulic
275 conductivity values in excess of 10^{-3} cm/s (1 darcy) decreased by two orders of magnitude. During this
276 same period, measured flow rates decreased from >1 m/d to just over 0.1 m/d, after which the soil
277 around Profile 1 piezometers transitioned from saturated to unsaturated conditions. Saturated hydraulic
278 conductivity declined by an order of magnitude at the same time along Profile 4, but there was a
279 simultaneous (and proportionately larger) increase in the head gradient along this profile (Figure 4c),
280 which explains why the infiltration rate increased at the same time (Figure 4a). Once again, data from
281 Profile 2 indicate intermediate conditions, both a lower initial saturated hydraulic conductivity, and a
282 smaller decrease with time during the first 70 days of MAR operation.

Saturated hydraulic conductivity could not be determined for Profile 1 after ~60 days of MAR operation and for Profile 2 after 120 days of MAR operation because unsaturated conditions "decoupled" the hydrostatic head at the base of the pond from the partly drained soil below the inverted water table, preventing reliable application of Darcy's law. Unsaturated conditions were readily apparent on both pressure and temperature records recovered from PVC tubes along these profiles, creating pressure values ≤0 kPa (relative to atmospheric) and diel temperature oscillations having a much higher amplitude than those measured when temperature sensors were in a fluid-filled tube.

Discussion and Conclusions

We were surprised by the extent of spatial and temporal variability in infiltration rates documented in this study. Our initial assessment of shallow soils was that they were relatively homogeneous, being mainly silty sand, but relatively small differences in the percentage of fine material can have a large influence on saturated hydraulic conductivity, and on saturation and drainage properties. The significance of variable infiltration is most apparent when temporal data from the HS-MAR pond are contoured and viewed as a function of time since the start of MAR operations (Figure 5). The most rapid infiltration occurred initially near the northwestern side of the pond, but infiltration rates in this area decreased at the same time that infiltration rates increased near the southeastern side of the pond. In effect, the locus of the fastest infiltration, which would contribute most to increasing the saturation of underlying soils (and presumably to recharging the underlying aquifer), swept across the pond from northwest to southeast. The center of the most rapid infiltration migrated at a time-averaged rate of ~2 m/d, before dissipating late in the MAR operating season. These changes in infiltration rates were often associated with quantitative changes in saturated hydraulic conductivity.

Like many such systems, the HS-MAR pond accumulates fine grained sediments during each period of system operation. Sources of sediment to the pond may include the suspended load in diverted water

309 (generally kept low by filtering during diversion), hill-slope erosion, and overflow from adjacent
310 agricultural fields during large precipitation events. The HS-MAR pond is scraped at the end of each
311 operating season to restore rapid infiltration properties, and additional work is needed to asses the extent
312 to which lower infiltration rates, and disparate patterns of falling and rising saturated hydraulic
313 conductivity, may result from sediment accumulation, sediment penetration, or biofouling. Similarly,
314 work is needed to assess whether the initial rise in saturated hydraulic conductivity in shallow soils
315 (Figure 4d) resulted main from establishment and deepening of the shallow water table, flushing of fine
316 grains from soil pores, or other processes.
317
318 Hydrologists have used the variable source area (VSA) concept for decades to understand spatial and
319 temporal patterns of catchment runoff (Dunne and Black 1970; Hoover 1990; Quinn and Beven 1993).
320 The VSA concept is based on the observation that different parts of a catchment can contribute different
321 amounts of runoff at different times during precipitation events. The present study suggests that the
322 variable source concept might be usefully extended to infiltration (and perhaps groundwater recharge as
323 well), as a framework for describing and understanding spatial and temporal variability. The lateral
324 migration of the infiltration peak was assessed using data collected from mainly the upper ~1 m of soil
325 below this MAR pond, but we have not presented information on deeper conditions and processes.
326 Additional investigation, water chemical analyses, and modeling will be necessary to assess the extent
327 to which spatial and temporal patterns of shallow infiltration were expressed as groundwater recharge at
328 depth.
329
330 Quantifying the nature, spatial extent, and temporal development of decreases in hydraulic conductivity
331 at the base of MAR ponds is a crucial step in designing and operating these systems so as to maximize
332 benefit to limited (and often fragile) aquatic resources. In the present case, options are being explored
333 for reducing sediment load into the pond in an effort to maintain operational efficiency for a longer time
334 during the MAR season. Additional studies are underway to link local infiltration rates to changes in

nitrate load (Schmidt et al., 2011), which could be important for understanding why some recharge systems are more effective than others in improving water quality. Studies of MAR ponds also present opportunities to quantify and understand linked physical, chemical, and biological processes that may occur during infiltration and recharge in general. It remains to be determined if the variable infiltration area concept documented in the HS-MAR pond might apply to other MAR systems and within natural catchments more broadly. The use and comparison of system averaged and point-specific tools for measuring infiltration processes and properties across a range of spatial and temporal scales will allow a broader assessment of these conditions and their impacts on water resources.

ACKNOWLEDGMENTS

We thank the Pajaro Valley Water Management Agency for their prescient stewardship, and cooperative and collaborative efforts, in operating and providing access to the Harkins Slough Managed Aquifer Recharge system. We are grateful for technical and field support provided by Dan Sampson, Rob Franks, Bruce Daniels, Nic Massetani, and Joanna Hoffman. Heather Savage, Nicholas van der Elst, and Emily Brodsky helped with acquisition and processing of LiDAR data to produce the DEM. This research was financed by graduate fellowships from the Science, Technology, Engineering, Policy and Society Institute at UC Santa Cruz and the US Environmental Protection Agency, and grants from the UC Santa Cruz Committee on Research, the California Water Resources Control Agency (through the Santa Cruz County Resource Conservation District, UCSC-PAJARO013107), and the National Institutes for Water Resources (08HQGR0054)

356 FIGURE CAPTIONS

357 **Figure 1.** Site maps. (a) Project location in central coastal California, U.S. HS-MAR = Harkins Slough
358 managed aquifer recharge system. (b) Inset aerial photo showing regional sloughs (wetlands) and
359 location of MAR pond. (c) Distribution of sampling and instrumentation locations in the MAR pond
360 presented in this study. Diverted slough water used for MAR enters the pond adjacent to location P2-B.
361 Soil samples were collected along Profiles 1 to 4, and at additional locations across the MAR pond.

362

363 **Figure 2.** Illustration of thermal method used to assess point-specific infiltration rates (Hatch et al.,
364 2006). (a) Three thermal loggers and one pressure logger are suspended within a PVC pipe, screened at
365 the base and sealed at top. (b) Raw thermal record for piezometer P2-B showing 15-minute data
366 collected when the piezometer was filled with water and the shallow subsurface sediments were fully
367 saturated. (c) Filtered thermal record for the same piezometer and time period, showing just the diurnal
368 signal. Note difference in temperature scale compared to panel (b), and amplitude reduction and phase
369 shift with depth below the base of the pond.

370

371 **Figure 3.** (a) Whole-pond average infiltration rates, derived from mass-balance calculations, plotted
372 with pond stage during the full 2008 operating season. (b) Linear regression of infiltration rate versus
373 stage for the first 40 days of (a). Infiltration and stage are positively correlated during this period.

374

375 **Figure 4.** Plots of (a) thermally-derived infiltration rates, (b) subsurface pressure, (c) head gradient, and
376 (d) saturated hydraulic conductivity within the upper 1 m of soil below the base of the MAR infiltration
377 pond, for locations P1-C, P2-B and P4-D. Measurement locations shown in Figure 1C. Whole-pond
378 specific infiltration rate and 8-piezometer average rate are plotted for comparison in (a). Pond stage is
379 plotted for reference in (b) through (d). Data sets (a) and (d) were calculated as daily means, then
380 smoothed using a 7-day moving average.

381

382 **Figure 5.** Posted contour plots (hand-drawn) showing rates and the spatial distribution of infiltration at
383 15-day intervals during the first 80 days of the 2008 Harkins Slough MAR operating season. Contours
384 that extend beyond the posted data values are extrapolated, but the transition in infiltration rates near the
385 central part of the pond is well defined by the data.

386

387

388

389 REFERENCES

390 Anderson, M. P. 2005. Heat as a ground water tracer. *Ground Water* 43 (6):951-968.

391 Bouwer, H. 2002. Artificial recharge of groundwater: hydrogeology and engineering. *Hydrogeology*
392 *Journal* 10 (1):121-142.

393 Bouwer, H., J. Ludke, and R. C. Rice. 2001. Sealing pond bottoms with muddy water. *Ecological*
394 *Engineering* 18 (2):233-238.

395 California Water Plan Update. 2009. California Department of Water Resources.

396 Cardenas, M. B. 2010. Thermal skin effect of pipes in streambeds and its implications on groundwater
397 flux estimation using diurnal temperature signals. *Water Resources Research* 46.

398 Constantz, J., D. Stonestrom, A. E. Stewart, R. Niswonger, and T. R. Smith. 2001. Analysis of
399 streambed temperatures in ephemeral channels to determine streamflow frequency and duration.
400 *Water Resources Research* 37 (2):317-328.

401 Constantz, J., C. L. Thomas, and G. Zellweger. 1994. Influence of diurnal variations in stream
402 temperature on streamflow loss and groundwater recharge. *Water Resources Research* 30
403 (12):3253-3264.

404 Dunne, T., and R. D. Black. 1970. Partial area contributions to storm runoff in a small New England
405 watershed. *Water Resources Research* 6 (5):1296-&.

406 Fleckenstein, J., M. Anderson, G. Fogg, and J. Mount. 2004. Managing surface water-groundwater to
407 restore fall flows in the Cosumnes River. *Journal of Water Resources Planning and*
408 *Management-Asce* 130 (4):301-310.

409 Gallardo, A. H., A. Marui, S. Takeda, and F. Okuda. 2009. Groundwater supply under land subsidence
410 constrains in the Nobi Plain. *Geosciences Journal* 13 (2):151-159.

411 Greskowiak, J., H. Prommer, G. Massmann, C. D. Johnston, G. Nutzmann, and A. Pekdeger. 2005. The
412 impact of variably saturated conditions on hydrogeochemical changes during artificial recharge
413 of groundwater. *Applied Geochemistry* 20 (7):1409-1426.

414 Hanson, R. T. 2003. Geohydrologic Framework of Recharge and Seawater Intrusion in the Pajaro
415 Valley, Santa Cruz and Monterey Counties, California. Sacramento, CA: U. S. Geological
416 Survey.
417 Harou, J. J., and J. R. Lund. 2008. Ending groundwater overdraft in hydrologic-economic systems.
418 *Hydrogeology Journal* 16 (6):1039-1055.
419 Harvey, F. E., J. F. Ayers, and D. C. Gosselin. 2007. Ground water dependence of endangered
420 ecosystems: Nebraska's eastern saline wetlands. *Ground Water* 45 (6):736-752.
421 Hatch, C. E., A. T. Fisher, J. S. Revenaugh, J. Constantz, and C. Ruehl. 2006. Quantifying surface
422 water-groundwater interactions using time series analysis of streambed thermal records: Method
423 development. *Water Resources Research* 42 (10).
424 Hatch, C. E., A. T. Fisher, C. R. Ruehl, and G. Stemler. 2010. Spatial and temporal variations in
425 streambed hydraulic conductivity quantified with time-series thermal methods. *Journal of*
426 *Hydrology* 389 (3-4):276-288.
427 Heilweil, V. M., D. K. Solomon, and P. M. Gardner. 2007. Infiltration and recharge at Sand Hollow, an
428 upland bedrock basin in Southwestern Utah. In *Ground-Water Recharge in the Arid and*
429 *Semiarid Southwestern United States*, edited by D. A. Stonestrom, J. Constantz, T. P. A. Ferre
430 and S. A. Leake. Reston, VA: U. S. Geological Survey.
431 Hoover, J. R. 1990. Seep and runoff detector design and performance to determine extent and duration
432 of seep runoff zone from precipitation on hillsides. *Transactions of the Asae* 33 (6):1843-1850.
433 Izbicki, J. A., A. L. Flint, and C. L. Stamos. 2008. Artificial recharge through a thick, heterogeneous
434 unsaturated zone. *Ground Water* 46 (3):475-488.
435 Massmann, G., J. Sultenfuss, U. Dunnbier, A. Knappe, T. Taute, and A. Pekdeger. 2008. Investigation
436 of groundwater a residence times during bank filtration in Berlin: multi-tracer approach.
437 *Hydrological Processes* 22 (6):788-801.

438 Prommer, H., and P. J. Stuyfzand. 2005. Identification of temperature-dependent water quality changes
439 during a deep well injection experiment in a pyritic aquifer. *Environmental Science &*
440 *Technology* 39 (7):2200-2209.
441 Quinn, P. F., and K. J. Beven. 1993. Spatial and temporal predictions of soil-moisture dynamics, runoff,
442 variable source areas and evapotranspiration for Plynlimon, Mid-Wales. *Hydrological Processes*
443 7 (4):425-448.
444 Reinelt, P. 2005. Seawater intrusion policy analysis with a numerical spatially heterogeneous dynamic
445 optimization model. *Water Resources Research* 41 (5).
446 Ronan, A. D., D. E. Prudic, C. E. Thodal, and J. Constantz. 1998. Field study and simulation of diurnal
447 temperature effects on infiltration and variably saturated flow beneath an ephemeral stream.
448 *Water Resources Research* 34 (9):2137-2153.
449 Scanlon, B. R., R. W. Healy, and P. G. Cook. 2002. Choosing appropriate techniques for quantifying
450 groundwater recharge. *Hydrogeology Journal* 10 (1):18-39.
451 Schmidt, C. S., A. T. Fisher, A. Racz, C. G. Wheat, M. Los Huertos, and B. Lockwood. 2011. Rapid
452 nutrient load reduction during infiltration of managed aquifer recharge in an agricultural
453 groundwater basin. *Hydrological Processes, in press*.
454 Werner, A. D., and C. T. Simmons. 2009. Impact of Sea-Level Rise on Sea Water Intrusion in Coastal
455 Aquifers. *Ground Water* 47 (2):197-204.
456 Zektser, S., H. A. Loaiciga, and J. T. Wolf. 2005. Environmental impacts of groundwater overdraft:
457 selected case studies in the southwestern United States. *Environmental Geology* 47 (3):396-404.

458

459

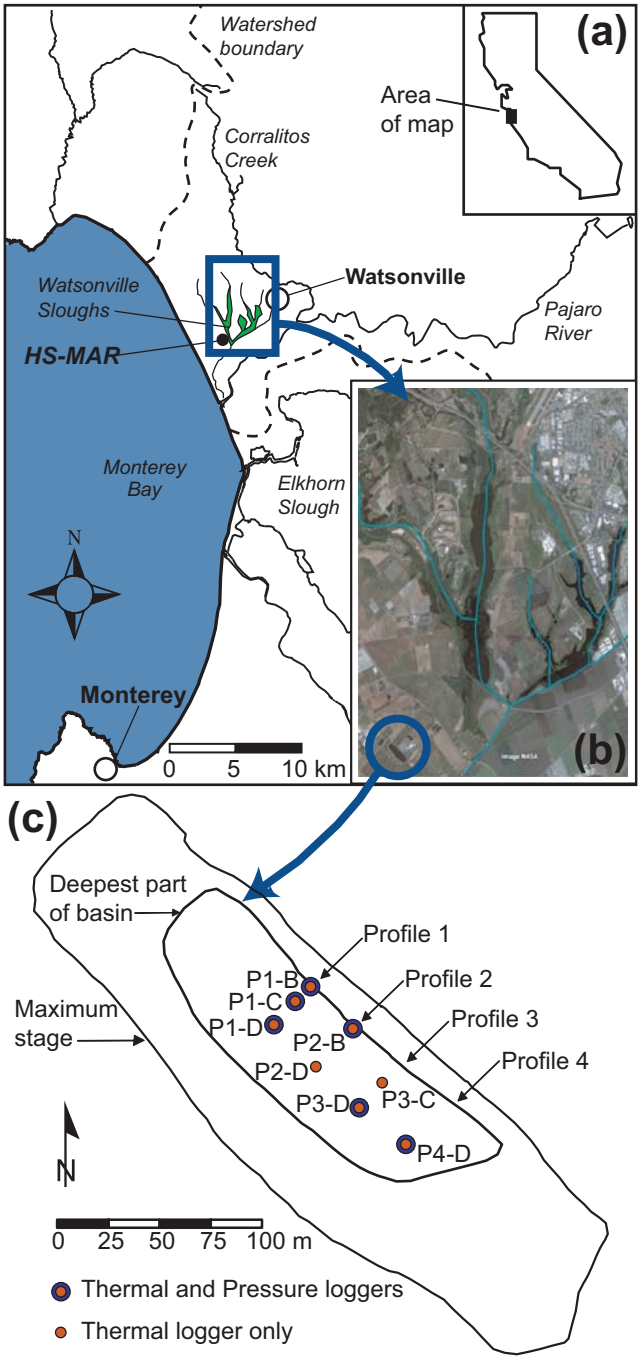
(a)
Watershed boundary
Area of map
Corralitos Creek
Watsonville
Watsonville Sloughs
HS-MAR
Pajaro River
Monterey Bay
Elkhorn Slough
N
Monterey
0 5 10 km
(b)
(c)
Deepest part of basin
Profile 1
P1-B
Profile 2
P1-C
Profile 3
P1-D
P2-B
Profile 4
Maximum stage
P2-D
P3-D
P3-C
P4-D
N
0 25 50 75 100 m
Thermal and Pressure loggers
Thermal logger only

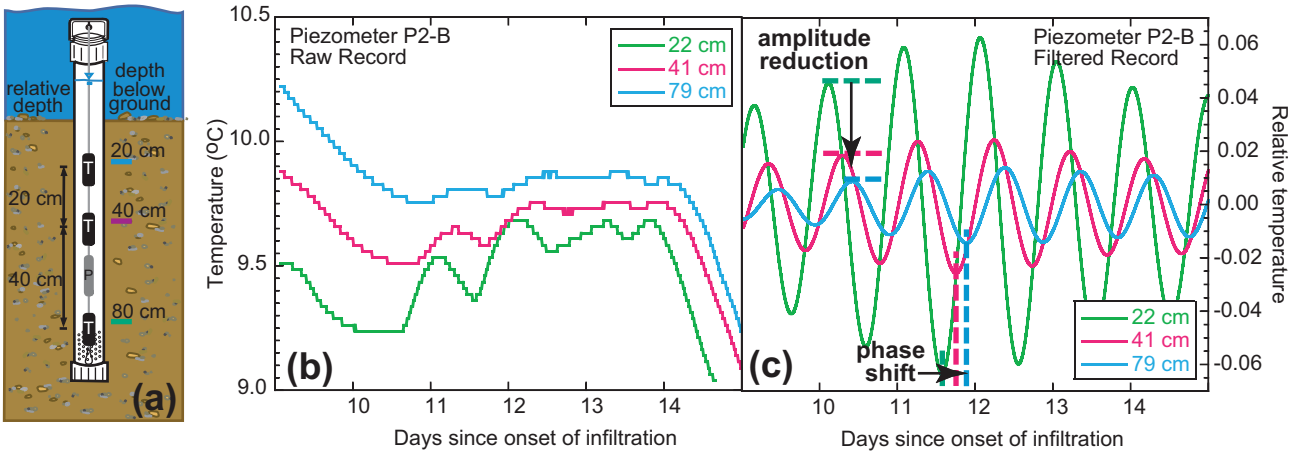
relative depth
depth below ground
20 cm
40 cm
80 cm
20 cm
40 cm
(a)
Piezometer P2-B
Raw Record
22 cm
41 cm
79 cm
Temperature (°C)
10.5
10.0
9.5
9.0
(b)
10
11
12
13
14
Days since onset of infiltration
amplitude reduction
phase shift
Piezometer P2-B
Filtered Record
(c)
0.06
0.04
0.02
0.00
-0.02
-0.04
-0.06
Relative temperature
Days since onset of infiltration

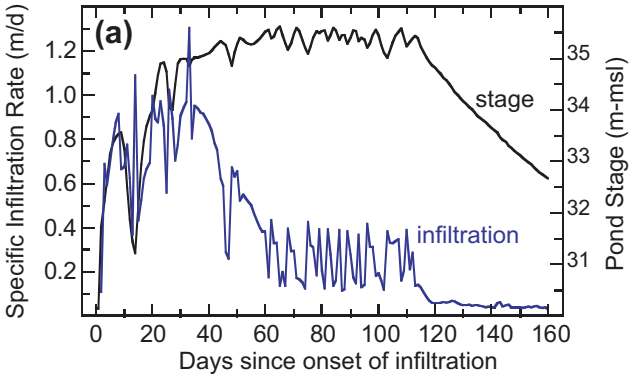
(a)
Specific Infiltration Rate (m/d)
Pond Stage (m-msl)
stage
infiltration
Days since onset of infiltration

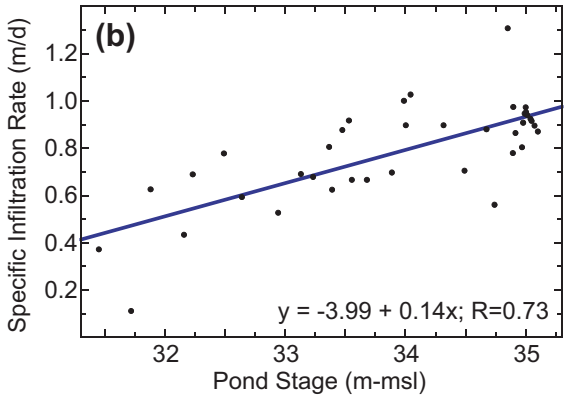
(b)
Specific Infiltration Rate (m/d)
y = -3.99 + 0.14x; R=0.73
Pond Stage (m-msl)

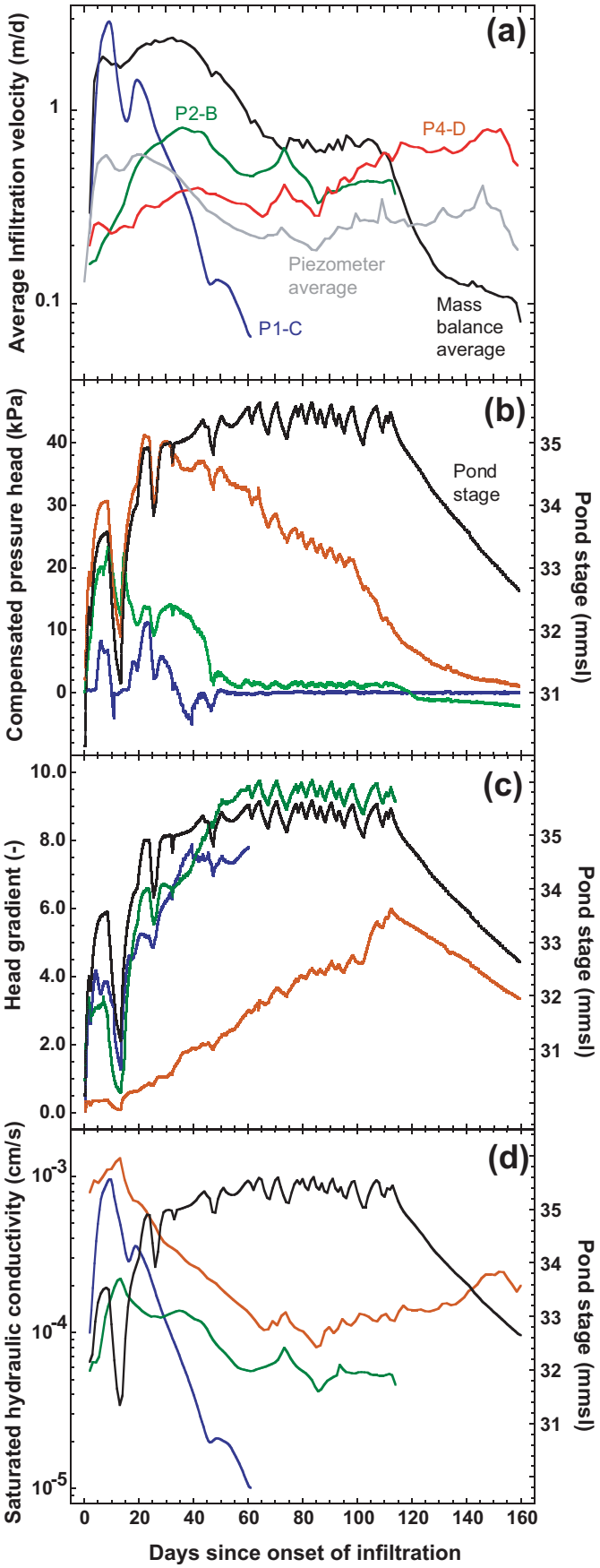
(a)
Average Infiltration velocity (m/d)
1
0.1
P2-B
P4-D
Piezometer
average
Mass
balance
average
P1-C
(b)
Compensated pressure head (kPa)
40
30
20
10
0
Pond
stage
35
34
33
32
31
Pond stage (mmsl)
(c)
Head gradient (-)
10.0
8.0
6.0
4.0
2.0
0.0
35
34
33
32
31
Pond stage (mmsl)
(d)
Saturated hydraulic conductivity (cm/s)
10-3
10-4
10-5
35
34
33
32
31
Pond stage (mmsl)
0
20
40
60
80
100
120
140
160
Days since onset of infiltration

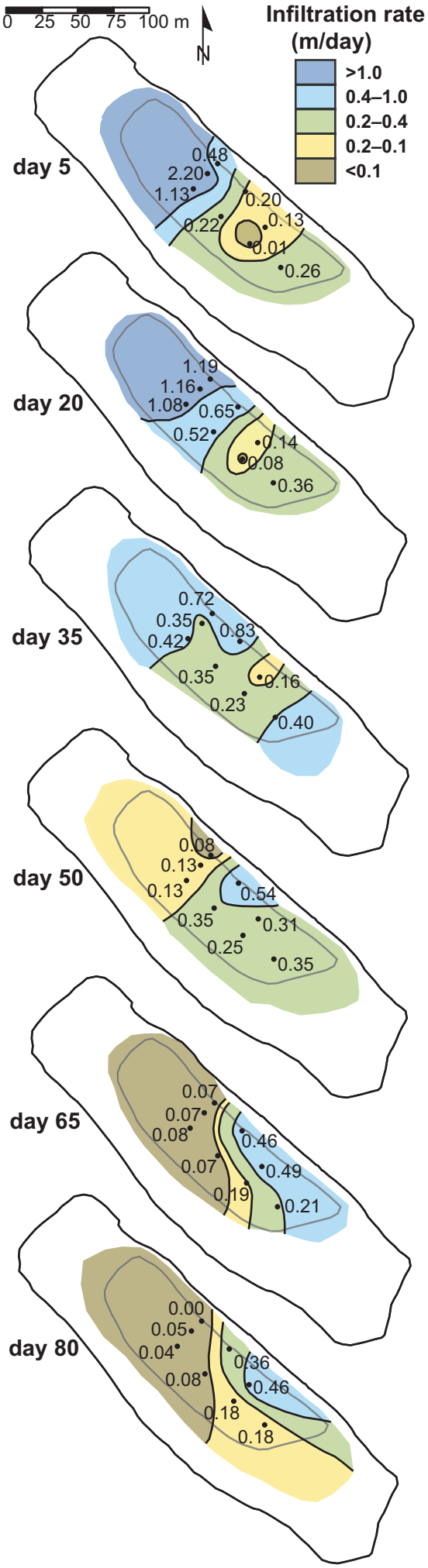
0 25 50 75 100 m
N
Infiltration rate (m/day)
>1.0
0.4–1.0
0.2–0.4
0.2–0.1
<0.1
day 5
0.48
2.20
1.13
0.20
0.22
0.13
0.01
0.26
day 20
1.19
1.16
1.08
0.65
0.52
0.14
0.08
0.36
day 35
0.72
0.35
0.42
0.83
0.35
0.16
0.23
0.40
day 50
0.08
0.13
0.13
0.54
0.35
0.31
0.25
0.35
day 65
0.07
0.07
0.08
0.46
0.07
0.49
0.19
0.21
day 80
0.00
0.05
0.04
0.36
0.08
0.46
0.18
0.18